Luminescent Eu^{3+} doped $NaLa(WO_4)(MoO_4)$ and Ba_2CaMoO_6 prepared by the modified Pechini method

M. Sletnes,[a] S. L. Skjærvø[a], M. Lindgren[b], T. Grande[a] and M-A. Einarsrud[a*]

[a] Department of Materials Science and Engineering, Norwegian University of Science and Technology, NO-7491 Trondheim, Norway

[b] Department of Physics, Norwegian University of Science and Technology, NO-7491 Trondheim, Norway

*Corresponding author: mari-ann.einarsrud@ntnu.no, +47 73594002

Abstract

Modified Pechini synthesis routes were developed for synthesis of the novel red phosphor materials $NaLa(WO_4)(MoO_4):Eu^{3+}$ and $Ba_2CaMoO_6:Eu^{3+}$. Phase pure $NaLa(WO_4)(MoO_4):Eu^{3+}$ was obtained at calcination temperatures ≥ 600 °C using malic acid or tartaric acid as complexing agents. Phase pure $Ba_2CaMoO_6:Eu^{3+}$ was attained using EDTA and citric acid, at calcination temperatures ≥ 800 °C. Choice of complexing agents were discussed on the basis of the solubility of the precursors, metal complex stability constants and conformations of the complexes. The powder properties were characterised using X-ray diffraction, thermal analysis and electron microscopy. Photoluminescence emission intensity was studied as a function of the complexing agents used and calcination temperature of the powders. Maximum emission intensity for $NaLa(WO_4)(MoO_4):Eu^{3+}$ was obtained at a calcination temperature of 600 °C, whereas the maximum for $Ba_2CaMoO_6:Eu^{3+}$ was obtained after calcination at 1100 °C. Both materials displayed desirable optical properties for use as phosphors in white light emitting diodes.

Keywords

Pechini, phosphor, WLED, Ba_2CaMoO_6, $NaLa(WO_4)(MoO_4)$, photoluminescence

1 Introduction

Development of new or improved synthesis routes to functional materials is important for the progress of sustainable energy technology. Wet chemical synthesis methods offer excellent control of important material properties, such as stoichiometry, homogeneity and crystal structure, as well as particle size and morphology, and are applicable to a wide range of materials. Here, a modified Pechini method is used to prepare phosphorescent oxides for application in white light emitting diodes (WLEDs).

WLEDs are very energy efficient compared to other white light sources, but "cold" light and poor colour rendering properties limit their attractiveness for general illumination. This can be improved by using a near ultraviolet (NUV) LED in combination with red, green and blue phosphors. Efficient green and blue phosphors already exist. However, the technology is limited by the lack of a stable and efficient red phosphor. A much researched group of novel red phosphor materials are the Eu^{3+} doped oxides of Mo and W, including compounds such as $Ca(W,Mo)O_4:Eu^{3+},Li^+$ [1,2], $M^+M^{3+}(WO_4)_{2-x}(MoO_4)_x:Eu^{3+}$ (M^+ = Li, Na, K; M^{3+} = La, Gd, Y, Lu, Bi) [3-5], $M_6(W,Mo)O_{12}:Eu^{3+}$ (M = Y, Gd, Lu)[6-9] and $AB(W,Mo)O_6:Eu^{3+}$ (A = Ca, Sr, Ba; B = Mg, Ca) [10-18]. The first two compounds crystallize in the scheelite structure, where there is enhancement of NUV excitation due to non-centrosymmetric lattice sites. $M_6(W,Mo)O_{12}:Eu^{3+}$ (M = Y, Gd, Lu) and $AB(W,Mo)O_6:Eu^{3+}$ (A = Ca, Sr, Ba; B = Mg, Ca) crystallize in structures with MoO_6 groups, where the NUV excitation is enhanced via energy transfer from the host material. The most common synthesis route for these materials is solid state reaction [3,11-13,17,10,19], mainly because of the simplicity of the method, such as no need for soluble precursors or advanced equipment. However, several grindings and re-firings are often necessary to achieve phase purity, and the process readily introduces impurities and defects which would reduce luminous efficacy [20].

Pechini-type sol-gel synthesis is highly suitable for fabrication of phosphor materials due to its versatility and ability to produce powders of high homogeneity and purity at relatively low temperatures. Thus, there are several reports of modified Pechini synthesis of scheelite structured molybdate/tungstate phosphor materials [21-26]. Zhang et al. synthesised 6-coordinated $(Sr_{0.98-x}Ba_xEu_{0.02})_2Ca(Mo_{1-y}W_y)O_6$ by a modified Pechini route, however, the Raman spectroscopy data strongly suggests that there were secondary phases present in the material [16]. Very recently, Li and Liu also reported synthesis of $Ba_2CaMoO_6:Eu^{3+}$ by a Pechini route using citric acid as a complexing agent and a calcination temperature of 1100 °C [27]. The paper focused more on optical properties than the actual synthesis. Thus optimisation of synthesis parameters was not discussed, and it is difficult to determine from the published data whether complete phase purity was obtained. Here we report the synthesis of phase pure $NaLa(WO_4)(MoO_4):Eu^{3+}$ and $Ba_2CaMoO_6:Eu^{3+}$ by the modified Pechini method, with optimisation of important synthesis parameters such as complexing agents, pH and calcination temperatures. The relationship between phase purity and complexing agents are discussed with a basis in metal complex stability constants and conformations of the complexes.

2 Experimental

2.1 Materials

All the precursors were bought from Sigma Aldrich. $La(NO_3)_3 \cdot 6\ H_2O$ (99.9 %), $Eu(NO_3)_3 \cdot 6H_2O$ (99.9 %), KNO_3 (≥ 99.0 %), H_2WO_4 (99.0 %), $(NH_4)_6Mo_7O_{24} \cdot 4H_2O$ (99.98 %), $Ca(NO_3)_2 \cdot 4H_2O$ (≥ 99.0 %), malic acid (MA, 99.0 %), DL-tartaric acid (TA, 99%), citric acid (CA, 99 %), ethylenediaminetetraacetic acid (EDTA, ≥ 99 %), diethylenetriaminepentaacetic acid (DTPA, ≥ 99.0 %) and ethylene glycol (EG, ≥ 99.5 %) were used without further purification. $NaNO_3$ (99.0 %) and $Ba(NO_3)_2$ (≥ 99 %) were dried at 200 °C for at least 12 h prior to use. The concentrations of cation precursor solutions were determined using thermogravimetric standardisation.

2.2 Synthesis of $NaLa(WO_4)(MoO_4):Eu^{3+}$

A flow chart of the synthesis route to $NaLa(WO_4)(MoO_4):Eu^{3+}$ is presented in Fig. 1. Precursor solutions of $La(NO_3)_3 \cdot 6H_2O$ (~ 0.3 mol La per g solution), H_2WO_4 (~ 0.2 mol W per g solution) and $(NH_4)_6Mo_7O_{24} \cdot 4H_2O$ (~ 0.6 mol Mo per g solution) complexed with MA or TA in a 1:1 ratio with the cations were prepared and

standardised. The tungstate solution was made with a basis in the route developed by Gil et al [28]. The precursor solutions were mixed in the order W (0.01 mol), Mo (0.01 mol) and then La (0.0096 mol). $NaNO_3$ (0.0096 mol) and $Eu(NO_3)_3 \cdot 6H_2O$ (0.0008 mol) were added along with an additional amount of complexing agent to give a cation to complexing agent ratio of 1:1. EG (0.04 mol) was added to some of the syntheses, as shown in Table 1. The solutions were heated to 100 °C on a hot-plate and as the water content became critically low, the gels self-ignited initiating smoldering reactions. The cool and dry gels were crushed into homogeneous powders in an agate mortar before they were calcined in air at 300, 400, 500, 600, 700 and 1000 °C.

Table 1 Combinations of complexing and polymerisation agents investigated in the synthesis of $NaLa(WO_4)(MoO_4):Eu^{3+}$

Complexing agent(s)	**Ethylene glycol**
Malic acid	No
Malic acid	Yes
Tartaric acid	No
Tartaric acid	Yes

2.3 Synthesis of $Ba_2CaMoO_6:Eu^{3+}$

A flow chart showing the synthesis of $Ba_2CaMoO_6:Eu^{3+}$ is given in Fig. 2. Preliminary experiments [29] were carried out without addition of the Eu^{3+} dopant in order to find suitable complexing agents, molar ratios of complexing agents to cations, pH values and calcination temperatures. The investigated complexing agents were MA, TA, CA, EDTA and DTPA. EG was used as a polymerization agent in some of the syntheses. The complexing agents were dissolved in water and the pH was adjusted with NH_3 solution (25 %). Stoichiometric amounts of $Ca(NO_3)_2 \cdot 4H_2O$ and $(NH_4)_6Mo_7O_{24} \cdot 4H_2O$ were added in the form of precursor solutions of approximately $5 \cdot 10^{-4}$ mol cations/g. $Ba(NO_3)_2$ was dissolved in the solution, EG was added, and the water was slowly evaporated at 120 °C on a hotplate until a viscous/sticky gel was obtained. The gel was partly decomposed at 200 °C for 12 h. The resulting materials were calcined in air at 550, 600, 700 or 1100 °C for 6 h. Based on the preliminary experiments, DTPA, CA, and CA in combination with either EDTA or DTPA were chosen for the synthesis of Eu^{3+} doped Ba_2CaMoO_6. An overview of the syntheses with pH values and complexing agent to cation ratio is shown in Table 2. EG was not used in any of the syntheses of Eu^{3+} doped samples.

Table 2 Combinations of complexing agents and pH values investigated in the synthesis of $Ba_2CaMoO_6:Eu^{3+}$

Complexing agent(s)	**Ratio to cations**	**pH**
CA, EDTA	2, 1	8.0
CA, DTPA	2, 1	8.0
DTPA	1	7.0

2.4 Characterisation

Thermogravimetric analysis (TGA) and differential scanning calorimetry (DSC) were performed on the ground gels (after smoldering) using a Netzsch STA 449C Jupiter in synthetic air. The $NaLa(WO_4)(MoO_4)$ gels were analysed up to 1000 °C with a heating rate of 10 °C/min. The Ba_2CaMoO_6 gels were analysed up to 1100 °C with a heating rate of 5 °C/min. The crystal structure and phase composition of the phosphors were studied by X-ray powder diffraction (XRD) using a Bruker AXS D8 Focus equipped with a LynxEye™ detector and a Cu-radiation source ($CuK\alpha_{1,2}$) with Bragg Brentano geometry. Crystallite sizes were estimated from the XRD data using the Scherrer equation.[30] Scanning electron microscopy (SEM) was performed in a Hitachi S-5500 S (in-lens) ultra high resolution S(T)EM. BET surface area was calculated from nitrogen gas adsorption (Micromeritics Tristar 3000) on powder samples. The average particle sizes of the powders were estimated from

the BET surface areas by assuming spherical particles. Photoluminescence (PL) excitation and emission spectra were measured using a Horiba Jobin-Yvon Fluorolog-3 spectrofluorimeter with a Xenon lamp as an excitation source and a model R928P (photomultiplier tube) Hamamatsu detector. The powders were pressed into discs with a diameter of 13 mm, and mounted on a custom made sample holder. Emission spectra used for comparing emission intensities were measured using a Leica DM5500 B fluorescence microscope equipped with an ASI hyperspectral imager. The emission of the samples were measured in random order on the same day, using the same settings, and integrated emission intensities were numerically calculated using the trapz function in Matlab.

3 Results

3.1 Powder properties

Single-phase Eu-doped $NaLa(WO_4)(MoO_4)$ powders were obtained for all the synthesis routes with calcination temperatures ≥ 600 ºC, as evidenced by XRD. The crystal structure was Scheelite ($I4_1/a$) with lattice parameters a = 5.341 and c = 11.695 Å, which is in good agreement with the literature on $NaLa(WO_4)_2$ (a = 5.349, b = 11.628 Å) [31] and $NaLa(MoO_4)_2$ (a = 5.342, b = 11.738) [32]. Evolution of the X-ray diffractograms with calcination temperature is shown in Fig. 3 for the synthesis with TA as a complexing agent. The same trend was found for all the other combinations of complexing agents, except using MA without EG, where precipitation of one or more crystalline phases occurred in the gel. The appearance of the crystalline compound(s) diminished significantly upon calcination at 300 °C. The crystalline phase(s) could not be identified, but the low decomposition temperature indicates that it was an organic salt. The diffractograms after calcination at 400 and 500 °C demonstrated formation of phase pure $NaLa(WO_4)(MoO_4)$. However, the grey colour of the powders as well as TGA indicated that the organic materials in the gel were not completely decomposed at these calcination temperatures. No substantial mass loss was observed by TGA after 600 °C for any of the gels. The crystallite sizes determined by the Scherrer equation were about 20, 30 and 45 nm after calcination at 600, 700 and 1000 °C, respectively.

Phase pure Ba_2CaMoO_6 was achieved with DTPA and with CA in combination with EDTA at a calcination temperature of 1100 °C, and thus these complexing agents were chosen for further development of the synthesis route. TGA and DSC of gels made with DTPA (1:1 ratio with cations), CA (3:1), and CA in combination with EDTA (2:1:1) are shown in Fig. 4. The main weight loss occurred below 550 °C, and was due to evaporation of absorbed water, and decomposition of the nitrates and organic gel network. The largest weight loss was accompanied by a sharp exothermic peak in the DSC curve, centred at 480 °C for CA, 510 °C for CA-EDTA, and 540 °C for DTPA, indicating the main combustion of the chelate complexes along with the formation of metal oxides. The final weight loss occurred between 710 and 770 °C, and was presumably related to decomposition of carbonate intermediates. The final weight loss occurred at a lower temperature for the CA-EDTA combination than for the other complexing agents. Although the TGA curve did not show any weight loss after 800 °C, the DSC curve indicated that an exothermic process was active until 1050 °C. This may be due to final ordering and crystallization of the perovskite material.

Fig. 5a shows the XRD patterns of 2 mol% Eu^{3+} doped Ba_2CaMoO_6 synthesised using DTPA (1:1 ratio with cations), CA in combination with EDTA (2:1:1) and CA in combination with DTPA (2:1:1) as complexing agents, calcined at 700, 800 and 1100 °C. The crystal structure of the main phase was cubic perovskite (Fm-3m) with lattice parameter a = 8.379 Å, corresponding well with published crystallographic data for Ba_2CaMoO_6 (a = 8.355 Å)[33].

A small amount of $BaMoO_4$ secondary phase was observed, evidenced by the reflection at $2\theta \approx 27$ ° for the samples calcined at 700 °C. However, all the syntheses except for the one with a combination of CA and DTPA yielded phase pure Ba_2CaMoO_6 after calcination at 800 and 1100 °C. Calcination of the precursor gels at 1100 °C resulted in higher phase purity than at 700 °C, but also significant grain growth and coarsening, as seen in the SEM images of Eu^{3+} doped Ba_2CaMoO_6 in Fig. 5 b and c. Estimated average particle size from BET surface area increased from 280 nm when the calcination temperature was 700 °C to 2.4 µm at 1100 °C.

3.2 Optical properties

The exciation and emission spectra of $NaLa(WO_4)(MoO_4)$:Eu^{3+} are shown in Fig. 6. The red area marks the wavelength range for NUV LED emission, and thus the range where the phosphor should easily be excited. The broad excitation band centred at ~260 nm is due to the O-W/Mo charge transfer. The other excitation peaks originate from the intra-configurational 4f–4f transitions of Eu^{3+} from the ground state $^7F_0$ to the excited states $^5D_4$,$^5L_6$ and $^5D_2$ [34]. The main emission line originates from the forced electric dipole transition, $^5D_0$ -$^7F_2$. Both the high relative intensity of the intra-configurational transitions of Eu^{3+} compared to the charge transfer (CT) band, and the domination of $^5D_0$-$^7F_2$ in the emission spectrum are clear evidence of Eu^{3+} in non-centrosymmetric lattice sites [35]. The integrated PL emission intensities of the 8 mol% Eu^{3+} doped $NaLa(WO_4)(MoO_4)$ is plotted as a function of calcination temperature in Fig. 7. The highest PL intensity was achieved for the powders calcined at 600 °C for both complexing agents, and the maximum intensity was slightly higher for tartaric acid than malic acid.

Fig. 8 displays the excitation and emission spectra of Ba_2CaMoO_6:Eu^{3+}. The broad MoO_6 charge transfer band in the ultraviolet allows efficient NUV excitation. Two main peaks were observed in the emission spectra, centred at 595 nm ($^5D_0$ -$^7F_1$) and 615 nm ($^5D_0$ -$^7F_2$). Transitions from $^5D_0$ to $^7F_3$ and $^7F_4$ were also noticeable as (very) weak emission peaks on the low energy side of the spectra. The dominating emission line originates from the magnetic dipole transition, $^5D_0$ -$^7F_1$, indicating Eu^{3+} in mainly centrosymmetric lattice sites. The integrated photoluminescence (PL) emission intensities of the 2 mol% Eu^{3+} doped Ba_2CaMoO_6 synthesized with different complexing agents is plotted as a function of calcination temperature in Fig. 9. No significant difference in emission intensity of the samples calcined at 700 and 800 °C was observed. However, calcination at 1100 °C led to a fourfold increase in emission intensity. The highest emission intensity was observed for the synthesis with a combination of CA and EDTA.

4 Discussion

Single-phase Eu-doped $NaLa(WO_4)(MoO_4)$ was produced with calcination temperatures as low as 600 °C, establishing the ease of making high quality powders with the modified Pechini method. All the complexing agents gave single phase materials at these temperatures. However, observation of crystalline phase(s) in the gels made with malic acid as the only complexing agent, suggests that tartaric acid or malic acid in combination with ethylene glycol are better choices for the synthesis of Eu-doped $NaLa(WO_4)(MoO_4)$.

The synthesis of Ba_2CaMoO_6 proved to be more challenging. Precipitation of $Ba(NO_3)_2$ was observed upon evaporation of water before gelation when MA or TA were used as complexing agents. Increasing the molar ratio of complexing agent to cations to 3:1 reduced the amount of precipitation, but did not completely eliminate it. When EDTA was used as the only complexing agent, XRD analysis of the gels also showed that precipitation had occurred. In this case, the precipitate was not readily identified, and was assumed to be an organic salt based on EDTA or its decomposition products. Adjusting the pH and EDTA to cation ratio did not eliminate the precipitation. CA (3:1 ratio with cations), DTPA (1:1) and CA and EDTA in combination (2:1:1) resulted in amorphous gels. None of the preliminary experiments yielded phase pure Ba_2CaMoO_6 after calcination at 550, 600 or 700 °C. Commonly observed secondary phases were $Ba_{1-x}Ca_xCO_3$ and $BaMoO_4$. Phase pure material was obtained by using either DTPA or EDTA in combination with CA and calcination temperatures ≥ 800 °C.

The difference in the required complexing agents for the synthesis of the two materials can be explained partly by the solubility of the precursors and stability of the cation complexes. The stability constants for complexes with Na^+, La^{3+}, Ca^2 and Ba^{2+} are plotted in Fig. 10. The stability constants are significantly higher for EDTA and DTPA than for MA, TA and CA, and the stability increases in the order Na^+<Ba^{2+}<Ca^{2+}<La^{3+}. Furthermore, the solubility of $NaNO_3$ is about 10 times higher than $Ba(NO_3)_2$, and hence strong complexation may not be necessary to avoid precipitation of $NaNO_3$. Thus it was possible to synthesise $NaLa(WO_4)(MoO_4)$ using weaker complexing agents than Ba_2CaMoO_6.

Phase pure Ba_2CaMoO_6 was only obtained with EDTA when in combination with CA, whereas DTPA resulted in phase pure material without addition of CA. Since EDTA is a hexadendate ligand, it can form up to 6 bonds with a metal cation. DTPA is potentially an octadentate ligand, but typically forms less than 8 bonds with most

metal cations, leaving one or two sites available for bonding with other reagents.[36,37] Hence this can explain why DTPA proved to be a better complexing agent than EDTA when not combined with CA.

There are several sol-gel syntheses of perovskites reported in the literature in which EDTA and CA are used in combination, and many of them involve basic cations, such as Sr, Ba and La [38-43]. The interaction of EDTA and CA is clearly favourable for the formation of metal-organic precursor gels for these perovskite materials, although the mechanism is not completely understood. It is interesting to note that the TGA of the Ba_2CaMoO_6 gels (Fig. 4) showed that the final weight loss occurred at a lower temperature for the EDTA-CA combination than for CA alone. It has previously been shown by Abdullah et al. that in the sol-gel synthesis of $BaCe_{0.54}Zr_{0.36}Y_{0.1}O_{2.95}$, gels prepared with an EDTA-CA combination exhibited lower thermal decomposition temperatures than gels prepared with EDTA or CA alone [38]. It was argued that the combination acted as a better combustion reagent to increase the reaction rate. As in our synthesis, Abdullah et al. did not observe any weight loss by TGA after 750 °C, but 1100 °C was necessary to obtain phase purity. Feldhoff et al. have shown that the synthesis of $(Ba_{0.5}Sr_{0.5})(Fe_{0.8}Zn_{0.2})O_{3-\delta}$ perovskites by the EDTA-CA sol-gel route involves nanoscale solid state reactions between carbonate and oxide intermediate phases [40]. This is in agreement with our observations of $BaCO_3$ and tetragonal molybdates for calcination temperatures ≤ 700 °C. The details of the reaction phases and mechanisms of such systems are highly complex, and the mixture of complexing agents could possibly be determining for the compositions of any nanoscale intermediate phases.

Based on the XRD and PL results, the synthesis route using a combination of EDTA and CA, and a calcination temperature of 1100 °C was the best choice for the synthesis of $Ba_2CaMoO_6:Eu^{3+}$. The fact that DTPA is a suspected human reproductive toxicant was also in favour of choosing the EDTA-CA route. Once the optimized synthesis parameters had been obtained for the synthesis of $Ba_2CaMoO_6:Eu^{3+}$, the synthesis route could easily be adapted to synthesise compounds in the Eu^{3+}-doped $(Sr,Ba)_2Ca(W,Mo)O_6$ series.

The emission of $NaLa(WO_4)(MoO_4):Eu^{3+}$, which was mainly concentrated at 615 nm, is perfect for phosphor converted WLEDs with high luminous efficiency [44]. However, the narrow lines in the NUV part of the excitation spectrum are not ideal for WLED application. The emission spectrum of the pumping LED changes slightly due to variations in the driving current and/or the junction temperature. To keep the emission colour of the WLED stable, it is important that the excitation spectrum of the phosphors are broad and flat enough to compensate for the variation in pumping wavelengths. It is very interesting to note that the highest PL emission intensity for $NaLa(WO_4)(MoO_4):Eu^{3+}$ was achieved at a calcination temperature of only 600 °C. This corresponds to the lowest calcination temperature which resulted in phase pure material, since the organic components of the gel were not completely decomposed at 500 °C. Usually one would expect the PL intensity to increase with increasing calcination temperature due to higher crystallinity and decreased surface area. The crystallite size after calcination at 600 °C was only about 20 nm, and the optical properties may be influenced by final size effects which are yet to be understood. A difference in absorption coefficients for the samples would also influence this result; however, we did not have the available equipment to measure this. Increased PL emission intensity in combination with smaller particle size is very interesting for WLED phosphors since using nanosized particles will eliminate efficiency loss due to scattering [20].

The excitation spectrum of $Ba_2CaMoO_6:Eu^{3+}$displayed a broad CT band in the NUV, and should thus provide the required emission stability under varying conditions. However, the main emission was concentrated at 595 nm, which does not give the optimal red colour purity for phosphor converted WLEDs. Substituting Sr for Ba results in lowering of the perovskite lattice symmetry, while substituting W for Mo broadens and shifts the CT band [17]. Thus playing with the composition could allow for optimisation of the optical properties. The modified Pechini synthesis route developed in this work would be ideal for such a task since it allows strict control of the stoichiometry, homogeneity and phase purity.

5 Conclusion

Phase pure $NaLa(WO_4)(MoO_4):Eu^{3+}$ and $Ba_2CaMoO_6:Eu^{3+}$ were synthesised by newly developed modified Pechini routes. Both materials displayed desirable optical properties for use as phosphors in WLEDS, and low calcination temperatures resulted in increased emission intensity for $NaLa(WO_4)(MoO_4):Eu^{3+}$. The different complexing agents chosen for the synthesis of the two materials was explained and discussed with respect to the

solubility of the precursors and stability of the cation complexes. This insight enables to simplify the design of modified Pechini routes to related oxide materials.

6 Acknowledgements

The work was funded by The Norwegian University of Science and Technology within the strategic research area MATERIALS.

7 References

1. Xie A, Yuan XM, Hai SJ, Wang JJ, Wang FX, Li L (2009) Enhancement emission intensity of $CaMoO_4$: Eu^{3+}, Na^+ phosphor via Bi co-doping and Si substitution for application to white LEDs. J Phys D: Appl Phys 42 (10):105107
2. Zhu CQ, Xiao SG, Ding BW, Yang XL, Qiang RF (2008) Synthesis and photoluminescent properties of Eu^{3+}-doped (1-x)CaO-xLi_2O-WO_3 phosphors. Mater Sci Eng, B 150 (2):95-98
3. Neeraj S, Kijima N, Cheetham AK (2004) Novel red phosphors for solid-state lighting: the system $NaM(WO_4)_{2-x}(MoO_4)_x$: Eu^{3+} (M=Gd, Y, Bi). Chem Phys Lett 387 (1-3):2-6
4. Li L, Zhang J, Zi W, Gan S, Ji G, Zou H, Xu X (2014) Synthesis and luminescent properties of high brightness $MRE(MoO_4)_2$:Eu^{3+} (M = Li, Na, K; RE = Gd, Y, Lu) red phosphors for white LEDs. Solid State Sci 29 (0):58-65
5. Li LL, Liu L, Zi WW, Yu H, Gan SC, Ji GJ, Zou HF, Xu XC (2013) Synthesis and luminescent properties of high brightness $MLa(WO_4)_2$:Eu^{3+} (M=Li, Na, K) and $NaRE(WO_4)_2$:Eu^{3+} (RE=Gd, Y, Lu) red phosphors. J Lumin 143:14-20
6. Li HY, Noh HM, Moon BK, Choi BC, Jeong JH, Jang K, Lee HS, Yi SS (2013) Wide-Band Excited $Y_6(WMo)_{0.5}O_{12}$:Eu Red Phosphor for White Light Emitting Diode: Structure Evolution, Photoluminescence Properties, and Energy Transfer Mechanisms Involved. Inorg Chem 52 (19):11210-11217
7. Li H, Yang HK, Moon BK, Choi BC, Jeong JH, Jang K, Lee HS, Yi SS (2011) Crystal Structure, Electronic Structure, and Optical and Photoluminescence Properties of Eu(III) Ion-Doped $Lu_6Mo(W)O_{12}$. Inorg Chem 50 (24):12522-12530
8. Li H, Yang HK, Moon BK, Choi BC, Jeong JH, Jang K, Lee HS, Yi SS (2011) Investigation of the structure and photoluminescence properties of Eu3+ ion-activated $Y_6W_xMo_{1-x}O_{12}$. J Mater Chem 21 (12):4531-4537
9. Tian Y, Chen BJ, Hua RN, Zhong HY, Cheng LH, Sun JS, Lu WL, Wan J (2009) Synthesis and characterization of novel red emitting nanocrystal Gd_6WO_{12}:Eu^{3+} phosphors. Physica B 404 (20):3598-3601
10. Ye S, Li YJ, Yu DC, Yang ZM, Zhang QY (2011) Structural effects on Stokes and anti-Stokes luminescence of double-perovskite $(Ba,Sr)_2CaMoO_6$: Yb^{3+}, Eu^{3+}. J Appl Phys 110 (1):013517
11. Sivakumar V, Varadaraju UV (2006) A Promising Orange-Red Phosphor Under Near UV Excitation. Electrochem Solid-State Lett 9 (6):H35-H38
12. Sivakumar V, Varadaraju UV (2007) An Orange-Red Phosphor under Near-UV Excitation for White Light Emitting Diodes. J Electrochem Soc 154 (1):J28-J31
13. Sivakumar V, Varadaraju UV (2008) Synthesis, phase transition and photoluminescence studies on Eu^{3+}-substituted double perovskites—A novel orange-red phosphor for solid-state lighting. J Solid State Chem 181 (12):3344-3351
14. Lei F, Yan B (2008) Synthesis and photoluminescence of perovskite-type Ca_2MgWO_6 : Eu^{3+} micrometer phosphor. J Optoelectron Adv Mater 10 (1):158-163
15. Li S, Wei XT, Deng KM, Tian XN, Qin YG, Chen YH, Yin M (2013) A new red-emitting phosphor of Eu^{3+}-doped $Sr_2MgMo_xW_{1-x}O_6$ for solid state lighting. Curr Appl Phys 13 (7):1288-1291
16. Zhang L, Han P, Han Y, Lu Z, Yang H, Wang L, Zhang Q (2013) Structure evolution and tunable luminescence of $(Sr_{0.98-m}Ba_mEu_{0.02})_2Ca(Mo_{1-n}W_n)O_6$ phosphor with ultraviolet excitation for white LEDs. J Alloys Compd 558 (0):229-235
17. Ye S, Wang CH, Liu ZS, Lu J, Jing XP (2008) Photoluminescence and energy transfer of phosphor series $Ba_{2-z}Sr_zCaMo_{1-y}W_yO_6$:Eu,Li for white light UVLED applications. Appl Phys B 91 (3-4):551-557
18. Ye S, Wang C-H, Jing X-P (2008) Photoluminescence and Raman Spectra of Double-Perovskite $Sr_2Ca(Mo/W)O_6$ with A- and B-Site Substitutions of Eu^{3+} J Electrochem Soc 155 (6):J148-J151
19. Wang Z, Liang H, Gong M, Su Q (2007) Luminescence investigation of Eu^{3+} activated double molybdates red phosphors with scheelite structure. J Alloys Compd 432 (1–2):308-312
20. Ye S, Xiao F, Pan YX, Ma YY, Zhang QY (2010) Phosphors in phosphor-converted white light-emitting diodes: Recent advances in materials, techniques and properties. Mater Sci Eng, R 71 (1):1-34
21. Zalga A, Moravec Z, Pinkas J, Kareiva A (2011) On the sol-gel preparation of different tungstates and molybdates. J Therm Anal Calorim 105 (1):3-11

22. Cao FB, Li LS, Tian YW, Chen YJ, Wu XR (2011) Investigation of red-emission phosphors (Ca,Sr)(Mo,W)O:Eu^{3+} crystal structure, luminous characteristics and calculation of Eu^{3+} $^5D_0$ quantum efficiency. Thin Solid Films 519 (22):7971-7976
23. Lei JL, Yu Y, Li LJ, Cheng SB, Li GY, Li NB (2012) Synthesis of $LiEu_{1-x}Bi_x(MoO_4)_2$ red phosphors by sol-gel method and their luminescent properties. J Rare Earths 30 (4):330-334
24. Cao F-B, Li L-S, Tian Y-W, Gao Z-F, Chen Y-J, Xiao L-J, Wu X-R (2011) Sol–gel synthesis of red-phosphors $[Na_xGd_{1-x/3-z}Eu_z]Mo_yW_{1-y}O_4$ powers and luminescence properties. Opt Mater 33 (6):751-754
25. Xie H, Li F, Xi H, Tian R, Wang X (2015) Luminescent properties of sol–gel processed red-emitting phosphor Eu^{3+}, Bi^{3+} co-doped (Ca,Sr)(Mo,W)O_4. J Mater Sci: Mater Electron 26 (1):23-31
26. Zhai Y, Li J, Li X, Dong Y, Wang Y, Song S (2015) Synthesis and luminescent properties of $NaLa(MoO_4)_2$:Eu^{3+},Tb^{3+} phosphors by microwave-assisted sol–gel method. J Sol-Gel Sci Technol 74 (2):544-549
27. Li Y, Liu X (2015) Energy transfer and luminescence properties of Ba_2CaMoO_6:Eu^{3+} phosphors prepared by sol–gel method. Opt Mater 42 (0):303-308
28. Gil V, Strom RA, Groven LJ, Einarsrud MA (2012) $La_{28-x}W_{4+x}O_{54+3x/2}$ Powders Prepared by Spray Pyrolysis. J Am Ceram Soc 95 (11):3403-3407
29. Sletnes M (2014) Wet chemical synthesis of silicon nanoparticles and phosphorescent oxides for white light emitting diodes. PhD Thesis, Norwegian University of Science and Technology, Trondheim
30. Patterson AL (1939) The Scherrer Formula for X-Ray Particle Size Determination. Phys Rev 56 (10):978-982
31. Li H, Hong G, Yue S (1990) Crystal study of $NaLn(WO_4)_2$ (Ln= La, Pr, Nd). Zhongguo Xitu Xuebao (J Chin Rare Earth Soc) 8:37-41
32. Teller R (1992) Refinement of some $Na_{0.5-x}M'_{0.5+x/3}[\ ]_{2x/3}MoO_4$, M' = Bi, Ce, La, scheelite structures with powder neutron and X-ray diffraction data. Acta Crystallogr C 48 (12):2101-2104
33. Steward EG, Rooksby HP (1951) Pseudo-cubic Alkaline-earth Tungstates and Molybdates of the R_3MX_6 Type. Acta Crystallogr 4 (6):503
34. Carnall WT, Fields PR, Rajnak K (1968) Electronic Energy Levels of Trivalent Lanthanide Aquo Ions .4. Eu3+. J Chem Phys 49 (10):4450-&
35. Ofelt GS (1962) Intensities of Crystal Spectra of Rare-Earth Ions. J Chem Phys 37 (3):511-520
36. Sadun C, Bucci R, Magri AL (2002) Structural analysis of the solid amorphous binuclear complexes of iron(III) and aluminum(III) with chromium(III)-DTPA chelator using energy dispersive X-ray diffraction. J Am Chem Soc 124 (12):3036-3041
37. Silva VL, Carvalho R, Freitas MP, Tormena CF, Melo WC (2007) Structural determination of Zn and Cd-DTPA complexes: MS, infrared, C-13 NMR and theoretical investigation. Spectrochim Acta A 68 (5):1197-1200
38. Abdullah NA, Hasan S, Osman N (2013 Article ID 908340) Role of CA-EDTA on the Synthesizing Process of Cerate-Zirconate Ceramics Electrolyte. J Chem:7
39. Ding XF, Liu YJ, Gao L, Guo L (2008) Synthesis and characterization of doped $LaCrO_3$ perovskite prepared by EDTA-citrate complexing method. J Alloys Compd 458 (1-2):346-350
40. Feldhoff A, Arnold M, Martynczuk J, Gesing TM, Wang H (2008) The sol-gel synthesis of perovskites by an EDTA/citrate complexing method involves nanoscale solid state reactions. Solid State Sci 10 (6):689-701
41. Jeong C, Ryu J, Noh T, Kim YN, Lee H (2013) Structural analysis and electrode performance of Ce doped $SrMnO_3$ synthesised by EDTA citrate complexing process. Adv Appl Ceram 112 (8):494-498
42. Patra H, Rout SK, Pratihar SK, Bhattacharya S (2011) Effect of process parameters on combined EDTA-citrate synthesis of $Ba_{0.5}Sr_{0.5}Co_{0.8}Fe_{0.2}O_{3-\delta}$ perovskite. Powder Technol 209 (1-3):98-104
43. Prasad DH, Park SY, Oh EO, Ji H, Kim HR, Yoon KJ, Son JW, Lee JH (2012) Synthesis of nano-crystalline $La_{1-x}Sr_xCoO_{3-\delta}$ perovskite oxides by EDTA-citrate complexing process and its catalytic activity for soot oxidation. Appl Catal, A 447:100-106
44. Smet PF, Parmentier AB, Poelman D (2011) Selecting Conversion Phosphors for White Light-Emitting Diodes. J Electrochem Soc 158 (6):R37-R54
45. Martell AE, Motekaitis RJ, Smith RM Critically selected stability constants of metal complexes database: Version 8. (NIST Database 46). Available for download at http://www.nist.gov/srd/nist46.cfm (May 4th 2014),

Figure Captions

Fig. 1 A flow chart of the synthesis route to $NaLa(WO_4)(MoO_4):Eu^{3+}$

Fig. 2 A flow chart of the synthesis route to Ba_2CaMoO_6

Fig. 3 XRD patterns of $NaLa(WO_4)(MoO_4):Eu^{3+}$ synthesised using tartaric acid as a complexing agent. Calcination temperatures are included in the figure

Fig. 4 TGA and DSC curves of Ba_2CaMoO_6 precursor gels with three different complexing agents

Fig. 5 XRD patterns of Ba_2CaMoO_6 synthesised by the modified Pechini method. Calcination temperatures and complexing agents are included in the figure, with the ratio of complexing agents to cations in parentheses. An asterisk indicates peaks originating from a $BaMoO_4$ secondary phase, and a reference pattern for Ba_2CaMoO_6 [33] is included. b) SEM images of $Ba_2CaMoO_6:Eu^{3+}$ powder produced by modified Pechini synthesis with CA and EDTA as complexing agents calcined at 700 and c) 1100 °C

Fig. 6 Excitation and emission spectrum of $NaLa(WO_4)(MoO_4):Eu^{3+}$. The red area marks the range for NUV LED emission. Contribution from the second order scattering of the emission grating is denoted with (*)

Fig. 7 Integrated PL emission intensities of the 8 mol% Eu^{3+} doped $NaLa(WO_4)(MoO_4)$ synthesized with different complexing agents as a function of calcination temperature. The excitation wavelength was 405 nm

Fig. 8 Excitation and emission spectrum of $Ba_2CaMoO_6:Eu^{3+}$. The red area marks the range for NUV LED emission. Contribution from the second order scattering of the emission grating is denoted with (*)

Fig. 9 Integrated PL emission intensities of the 2 mol% Eu^{3+} doped Ba_2CaMoO_6 synthesized with different complexing agents as a function of calcination temperature. The excitation wavelength was 405 nm

Fig. 10 Stability constants (log K) of complexes of Ca^{2+}, Ba^{2+}, Na^{+} and La^{3+} with malic acid, tartaric acid, citric acid, EDTA and DTPA. Based on data from reference [45]. The dotted lines are a guide to the eye

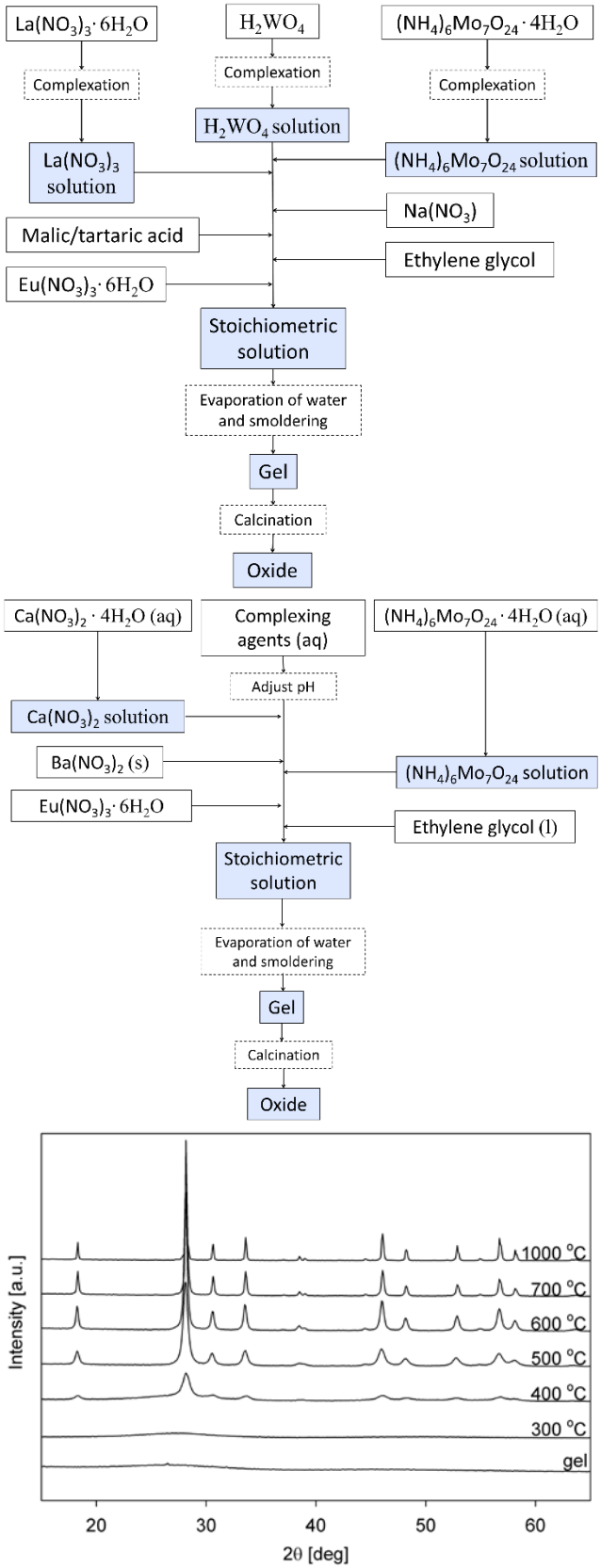
La(NO3)3· 6H2O
H2WO4
(NH4)6Mo7O24 · 4H2O
Complexation
Complexation
Complexation
H2WO4 solution
La(NO3)3 solution
(NH4)6Mo7O24 solution
Na(NO3)
Malic/tartaric acid
Ethylene glycol
Eu(NO3)3· 6H2O
Stoichiometric solution
Evaporation of water and smoldering
Gel
Calcination
Oxide
Ca(NO3)2 · 4H2O (aq)
Complexing agents (aq)
(NH4)6Mo7O24 · 4H2O (aq)
Adjust pH
Ca(NO3)2 solution
Ba(NO3)2 (s)
(NH4)6Mo7O24 solution
Eu(NO3)3· 6H2O
Ethylene glycol (l)
Stoichiometric solution
Evaporation of water and smoldering
Gel
Calcination
Oxide

Intensity [a.u.]
1000 °C
700 °C
600 °C
500 °C
400 °C
300 °C
gel
20
30
40
50
60
2θ [deg]

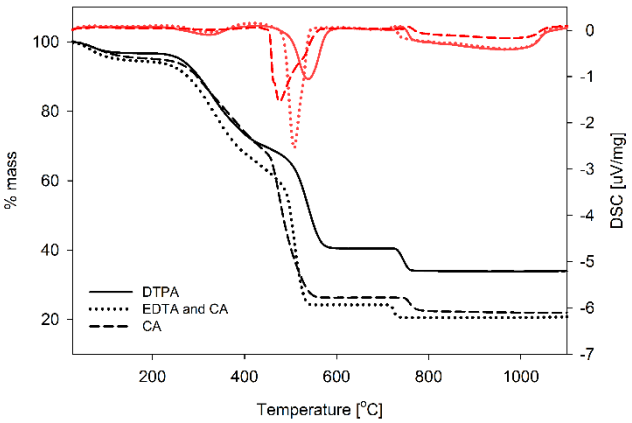
% mass
DSC [µV/mg]
Temperature [°C]
DTPA
EDTA and CA
CA

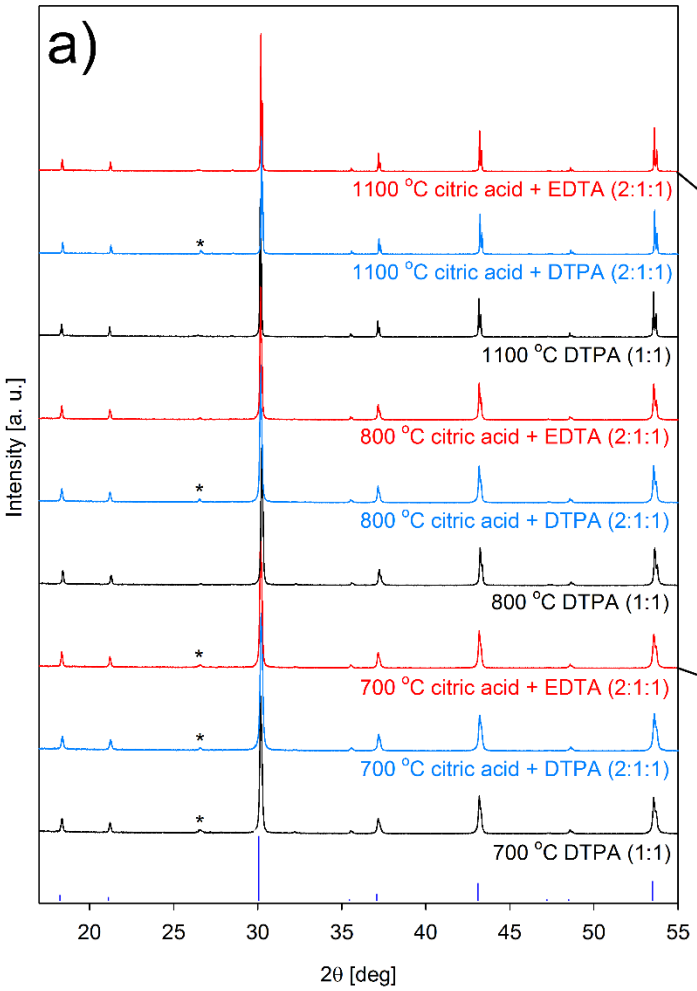
a)
1100 °C citric acid + EDTA (2:1:1)
1100 °C citric acid + DTPA (2:1:1)
1100 °C DTPA (1:1)
800 °C citric acid + EDTA (2:1:1)
800 °C citric acid + DTPA (2:1:1)
800 °C DTPA (1:1)
700 °C citric acid + EDTA (2:1:1)
700 °C citric acid + DTPA (2:1:1)
700 °C DTPA (1:1)
Intensity [a. u.]
2θ [deg]

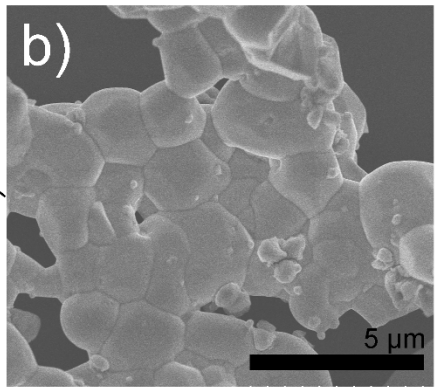
b)
5 µm

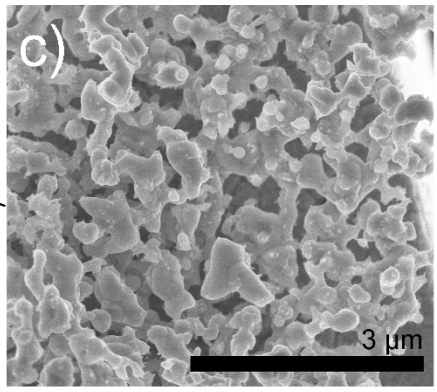
c)
3 µm

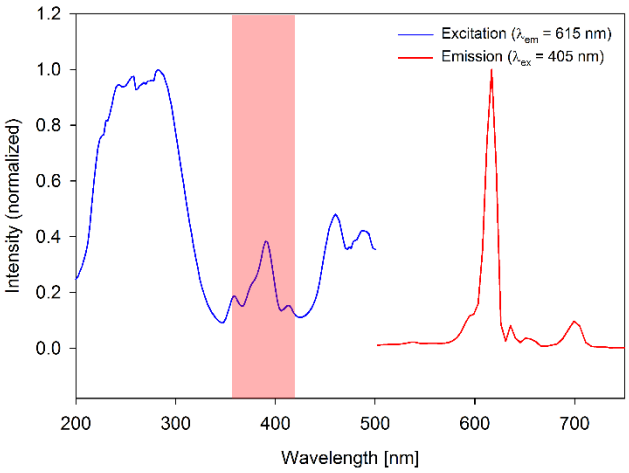
Excitation (λ_{em} = 615 nm)
Emission (λ_{ex} = 405 nm)
Intensity (normalized)
Wavelength [nm]

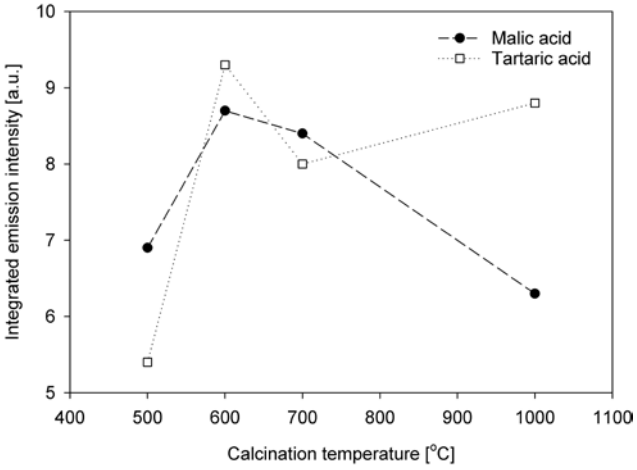
Malic acid
Tartaric acid
Integrated emission intensity [a.u.]
Calcination temperature [°C]

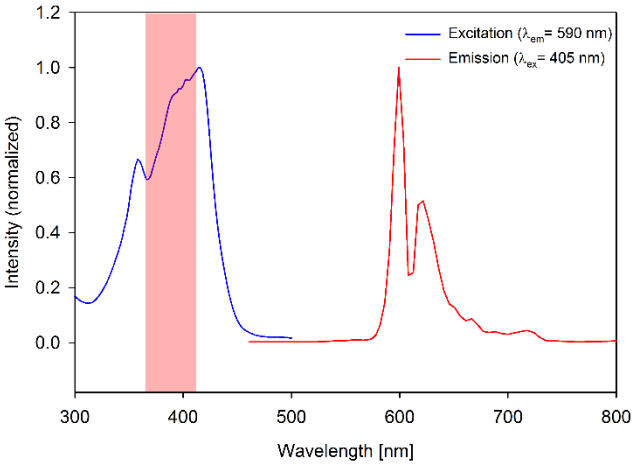
Excitation (λ_{em}= 590 nm)
Emission (λ_{ex}= 405 nm)
Intensity (normalized)
Wavelength [nm]

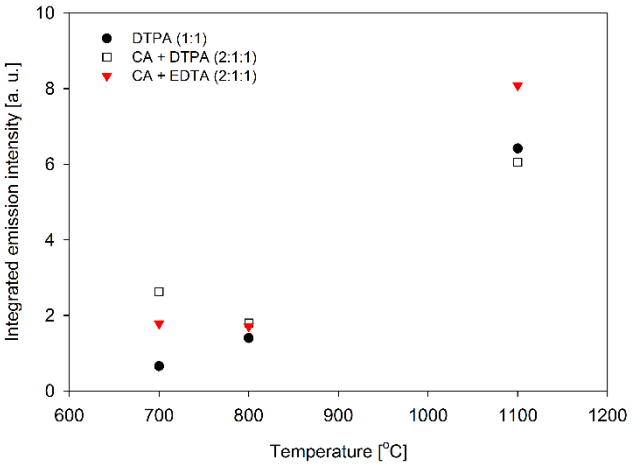
DTPA (1:1)
CA + DTPA (2:1:1)
CA + EDTA (2:1:1)
Integrated emission intensity [a. u.]
Temperature [°C]

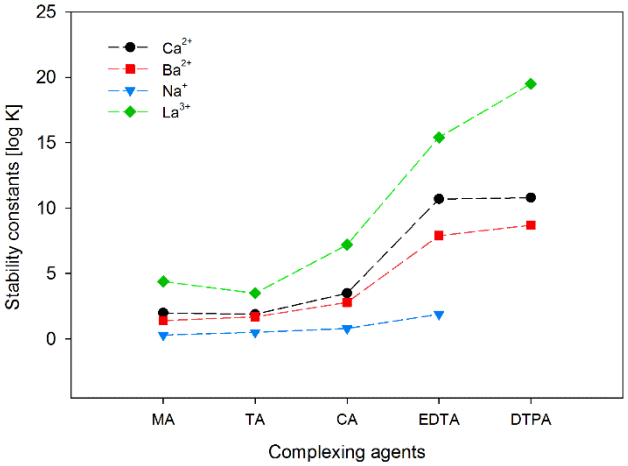
Ca2+
Ba2+
Na+
La3+
Stability constants [log K]
MA
TA
CA
EDTA
DTPA
Complexing agents